Eur. Phys. J. Special Topics **223**, 2527–2547 (2014)

DOI: 10.1140/epjst/e2014-02274-y

THE EUROPEAN PHYSICAL JOURNAL SPECIAL TOPICS

Regular Article

Supply networks: Instabilities without overload

Debsankha Manik[1,4], Dirk Witthaut[1,4,a], Benjamin Schäfer[1,3], Moritz Matthiae[1], Andreas Sorge[1], Martin Rohden[1], Eleni Katifori[1,2], and Marc Timme[1,2]

[1] Network Dynamics, Max Planck Institute for Dynamics and Self-Organization (MPI DS), 37077 Göttingen, Germany
[2] Faculty of Physics, University of Göttingen, 37077 Göttingen, Germany
[3] Otto-von-Guericke-Universität Magdeburg, 39106 Magdeburg, Germany
[4] These authors contributed equally to this work.

Received 19 March 2014 / Received in final form 30 July 2014
Published online 26 September 2014

Abstract. Supply and transport networks support much of our technical infrastructure as well as many biological processes. Their reliable function is thus essential for all aspects of life. Transport processes involving quantities beyond the pure loads exhibit alternative collective dynamical options compared to processes exclusively characterized by loads. Here we analyze the stability and bifurcations in oscillator models describing electric power grids and demonstrate that these networks exhibit instabilities without overloads. This phenomenon may well emerge also in other sufficiently complex supply or transport networks, including biological transport processes.

1 Introduction

Today's society depends on the reliable supply of electric power. The Energy transition to renewable energy (*Energiewende*) impairs the conventional power distribution system and poses great challenges for the security of the energy supply [1,2]. It has been shown by Pesch et al. [3] that the grid might become more heavily loaded in the future as electric power generation varies over time and has to be transported over large distances. For instance, current planning assigns new large-distance distribution lines from off-shore wind parks to the inner land – making the grid more susceptible to perturbations. Moreover, wind turbines and photovoltaic arrays are strongly intermittent; their power output fluctuates on all timescales from years to below seconds [4–6]. To ensure continued stable operation of power grids, it is advisable to understand how the network structure of the power grid determines its *dynamic* stability and how instabilities generally emerge.

[a] *Current address*: Forschungszentrum Jülich, Institute for Energy and Climate Research (IEK-STE), 52425 Jülich, Germany; e-mail: witthaut@nld.ds.mpg.de

2 An oscillator model for power grid operation

In this article we analyze network models of power grids consisting of rotating machines representing electric generators and motors. These models describe the *phase dynamics* of the machines and thus capture important problems of synchronization and dynamical stability of complex power grids [7–10] and have recently attracted considerable interest in physics and mathematics [11–16]. Notably, these models are mathematically very similar to the celebrated Kuramoto model describing the dynamics of coupled limit cycle oscillators [17–19].

Variations of these models are widely used in power engineering [7,8,10,20–22]. In many of the applications, however, passive loads are considered instead of motors which can be eliminated via a Kron reduction [23]. The resulting model is mathematical equivalent to the one analyzed here, but its dimension is typically significantly smaller *after this reduction* (see Sect. 2.2 for details).

2.1 The oscillator model

We model the power grid as a network of N rotating machines representing, for instance, wind turbines or electric motors [9,11]. Let the machines be denoted by a natural number $j \in Z_N$ where $Z_N = \{1, 2, \cdots, N\}$. Each machine j is characterized by the mechanical power P_j^{mech} it generates ($P_j^{\mathrm{mech}} > 0$) or consumes ($P_j^{\mathrm{mech}} < 0$). The state of each rotating machine is determined by its mechanical phase angle $\phi_j(t)$ and its velocity $d\phi_j/dt$. During the regular operation, generators as well as consumers within the grid run with the same frequency $\Omega = 2\pi \times 50\,\mathrm{Hz}$ (Europe) or $\Omega = 2\pi \times 60\,\mathrm{Hz}$ (USA). The phase of each element j is then written as

$$\phi_j(t) = \Omega t + \theta_j(t), \tag{1}$$

where θ_j denotes the phase difference to the reference value Ωt.

The equations of motion for all θ_j can now be obtained from the energy conservation law, i.e. the generated energy P_j^{mech} of each single element must equal the accumulated and dissipated mechanical energy of this machine plus the electric energy P_j^{el} transmitted to the rest of the grid. We also have

$$P_j^{\mathrm{diss}} = D_j(\dot{\phi}_j)^2 \tag{2}$$

$$P_j^{\mathrm{acc}} = \frac{1}{2} I_j \frac{d}{dt}(\dot{\phi}_j)^2, \tag{3}$$

where I_j is the moment of inertia and D_j is the damping torque. The energy conservation law reads

$$P_j^{\mathrm{mech}} = P_j^{\mathrm{diss}} + P_j^{\mathrm{acc}} + P_j^{\mathrm{el}}. \tag{4}$$

We will now insert equation (1) in the formula for the accumulated and dissipated mechanical energy to derive the equations of motion. In the vicinity of the regular operation of the grid, phase changes are small compared to the reference frequency [9] $|\dot{\theta}_j| \ll \Omega$ and we can write the equations of motion for θ_j as

$$\forall j \in Z_N, \quad I_j \Omega \ddot{\theta}_j = P_j^{\mathrm{mech}} - D_j \Omega^2 - 2D_j \Omega \dot{\theta}_j - P_j^{\mathrm{el}}. \tag{5}$$

The electric power is determined as follows. In a synchronous machine with p_f number of poles, the phase ϕ_j of the AC electric voltage and the mechanical phase ϕ_j^{mech} have a fixed ratio [20, p. 47]

$$\phi_j = \frac{p_f}{2} \phi_j^{\mathrm{mech}}.$$

We here consider common two-pole machines where this ratio is unity, i.e. $\phi_j(t) = \phi_j^{\mathrm{mech}}(t)$.

In an AC circuit, where the current between two nodes I_{ij} and voltage at jth node V_j vary sinusoidally with a relative phase difference δ, the power transmitted from node j to node i is

$$P_{ij}(t) = V_j(t) I_{ij}(t) \tag{6}$$

$$= \left(V_{j,\mathrm{rms}}\sqrt{2}\right) \sin(\Omega t) \left(I_{ij,\mathrm{rms}}\sqrt{2}\right) \sin(\Omega t + \delta) \tag{7}$$

$$= \underbrace{V_{j,\mathrm{rms}} I_{ij,\mathrm{rms}} \cos\delta}_{P_{ij,\mathrm{real}}} - V_{j,\mathrm{rms}} I_{ij,\mathrm{rms}} \cos(2\Omega t + \delta). \tag{8}$$

The second term oscillates between positive and negative values such that the direction of power flow changes direction. The net flow due to this term, when integrated over a full period of the AC cycle, is zero. Since here we consider dynamics on time scales much larger than a time period of the AC cycle ($1/\Omega$), we ignore this second term. The first term constitutes the *real power* flow from generator to consumers. It is convenient to adopt complex notation at this point:

$$\widetilde{V}_j = V_{j,\mathrm{rms}} e^{i\Omega t}, \quad \widetilde{I}_{ij} = I_{ij,\mathrm{rms}} e^{i(\Omega t + \delta)}, \tag{9}$$

such that the apparent and the real power reads

$$S_{ij} = \widetilde{V}_j \widetilde{I}_{ij}^*, \quad P_{ij,\mathrm{real}} = \Re(S_{ij}). \tag{10}$$

The net electric power at node j: P_j^{el} in (5) is basically the total P_{real} transmitted to all neighbouring nodes:

$$P_j^{\mathrm{el}} = \sum_{k=1}^{N} P_{kj,\mathrm{real}} \tag{11}$$

$$= \Re\left[\widetilde{V}_j \sum_{k=1}^{N} \widetilde{I}_{kj}^*\right] \tag{12}$$

$$\widetilde{I}_{kj} = Y_{kj}(\widetilde{V}_k - \widetilde{V}_j). \tag{13}$$

For simplicity we here neglect ohmic losses in the grid such that the admittance is purely imaginary, $Y_{jk} = iB_{jk}$. Furthermore, we assume that the magnitude of the voltage is constant throughout the grid, $|\widetilde{V}_j| = V_0$ for all nodes $j \in Z_N$. Then P_j^{el} simplifies to

$$P_j^{\mathrm{el}} = \Re\left[\sum_{k=1}^{N} V_0^2 B_{jk} \left\{\sin(\theta_j - \theta_k) + i\left(\cos(\theta_j - \theta_k) - 1\right)\right\}\right] \tag{14}$$

$$= \sum_{k=1}^{N} V_0^2 B_{jk} \sin(\theta_j - \theta_k). \tag{15}$$

Substituting this result into Eq. (5) thus yields the equations of motion

$$I_j \Omega \frac{d^2\theta_j}{dt^2} + D_j \frac{d\theta_j}{dt} = P_j^{\mathrm{mech}} - D_j\Omega^2 + \sum_{k=1}^{N} V_0^2 B_{jk} \sin(\theta_k - \theta_j). \tag{16}$$

The same equations of motions constitute the so-called structure-preserving model in power engineering [7], which is derived under slightly different assumptions.

For the sake of simplicity we introduce the abbreviations

$$P_j = \frac{P_j^{\mathrm{mech}} - D_j\Omega^2}{I_j\Omega} \tag{17}$$

$$\alpha_j = \frac{D_j}{I_j\Omega} \tag{18}$$

$$K_{jk} = \frac{V_0^2 B_{jk}}{I_j\Omega} \tag{19}$$

such that the equations of motion read

$$\forall j \in Z_N, \quad \frac{d^2\theta_j}{dt^2} = P_j - \alpha_j \frac{d\theta_j}{dt} + \sum_k K_{jk}\sin(\theta_k - \theta_j). \tag{20}$$

In this formulation the regular operation of the grid corresponds to a stable fixed point with $d\theta_j/dt = 0$ for all nodes j.

Throughout this paper we assume that the network defined by the coupling matrix is globally connected. Otherwise we can simply consider each connected component separately. We take symmetric transmission capacities

$$K_{jk} = K_{kj} \tag{21}$$

for all j, k as appropriate for (electric) supply networks and $K_{jj} = 0$. Furthermore, we assume that the power in the grid is balanced, i.e. $\sum_j P_j = 0$. This is appropriate since we focus on the short-time dynamics of the grid and the stability of steady states. On longer time-scales, the power balance is maintained by the grid operators by adapting the generation.

2.2 Ohmic loads and the classical model

The oscillator model introduced above assumes that all nodes of the network represent synchronous machines. In contrast, the so-called classical model widely studied in power engineering [10] includes a set of synchronous generators as above, but considers only ohmic loads. The load nodes of the network can then be eliminated which yields a much lower dimensional dynamical system. The resulting equations of motion are mathematically equivalent such that all our results equally well apply to the classical model. However, the network topology is no longer obvious in this model as the effective coupling matrix of the generator nodes is generally non-zero everywhere. Bergen and Hill [24] rectified this issue by introducing the *structure preserving model*, which also gives rise to equations of motion formally identical to the oscillator model. We thus focus on the oscillator model in the rest of the paper.

In the following we briefly summarize the derivation of the classical model [23] to show how to deal with ohmic loads in this framework. We divide the nodes of the networks into active and passive nodes, where the passive ones represent ohmic loads. For the sake of simplicity we label the nodes such that $j = 1, \ldots, L$ are the active nodes and $k = L+1, \ldots, N$ are the passive nodes. The passive nodes have a fixed power consumption

$$S_j = \widetilde{V}_j \underbrace{\sum_{k=1}^{N} \widetilde{I}_{kj}^*}_{=:\widetilde{I}_j^*}. \tag{22}$$

Even more, one assumes that both factors $\widetilde{V}_j$ and $\widetilde{I}_j$ are fixed independently. One can then eliminate these nodes via a Kron reduction as follows.

One starts with Kirchhoff's equations in the form (cf. Eq. (13))

$$\widetilde{I}_j = \sum_{k=1}^{N} \widetilde{I}_{jk} = \sum_k Y_{jk}(\widetilde{V}_k - \widetilde{V}_j) = \sum_k Q_{jk}\widetilde{V}_k, \tag{23}$$

where

$$Q_{jk} = Y_{jk} - \delta_{jk}\sum\nolimits_\ell Y_{j\ell} \tag{24}$$

is called *the nodal admittance matrix*. These equations are recast into matrix form

$$\begin{pmatrix} \boldsymbol{I}_a \\ \boldsymbol{I}_p \end{pmatrix} = \begin{pmatrix} Q_{aa} & Q_{ap} \\ Q_{pa} & Q_{pp} \end{pmatrix} \begin{pmatrix} \boldsymbol{V}_a \\ \boldsymbol{V}_p \end{pmatrix}, \tag{25}$$

where the vectors $\boldsymbol{I}_a$ and $\boldsymbol{I}_p$ collect the currents at the active and the passive nodes, respectively. These equations are solved for the currents

$$\boldsymbol{I}_a = \underbrace{(Q_{ap}Q_{pp}^{-1})}_{=:Q^{\mathrm{ac}}}\boldsymbol{I}_p + \underbrace{(Q_{aa} - Q_{ap}Q_{pp}^{-1}Q_{pa})}_{=:Q^{\mathrm{red}}}\boldsymbol{V}_a \tag{26}$$

at the active nodes. The net electric power at one of the active nodes then reads

$$S_j = \widetilde{V}_j \sum_{\ell=1}^{L} Q_{j\ell}^{\mathrm{red}*}\widetilde{V}_\ell^* + \widetilde{V}_j \sum_{\ell=L+1}^{N} Q_{j\ell}^{\mathrm{ac}*}\widetilde{I}_\ell^*. \tag{27}$$

The second term is fixed by assumption, such that it can be transfered to the effective mechanical power of the respective node,

$$P_j^{\mathrm{eff}} = P_j^{\mathrm{mech}} - \Re\left[\widetilde{V}_j \sum_{\ell=L+1}^{N} Q_{j\ell}^{\mathrm{ac}*}\widetilde{I}_\ell^*\right]. \tag{28}$$

Assuming again that the lines are lossless such that

$$Y_{jk} = iB_{jk} \qquad \text{and} \qquad Q_{j\ell}^{\mathrm{red}*} = iB_{j\ell}^{\mathrm{red}}, \tag{29}$$

the equations of motion for the active nodes are then derived from the energy conservation Eq. (4)

$$I_j\Omega\frac{d^2\theta_j}{dt^2} + D_j\frac{d\theta_j}{dt} = P_j^{\mathrm{eff}} - D_j\Omega^2 + \sum_{\ell=1}^{L} V_0^2 B_{j\ell}^{\mathrm{red}}\sin(\theta_\ell - \theta_j). \tag{30}$$

This is fully equivalent to the equations of motion for the oscillator model (16) such that all mathematical results obtained in the present article can thus be directly applied to the classical model as well.

2.3 Further generalisations

Both the oscillator and the classical model describe only the phase dynamics of the synchronous machines, assuming a constant voltage throughout the grid. Several important aspects of the voltage dynamics in a complex power grid are described by the so-called third-order model [10]. A recent theoretical study of voltage instabilities can be found in [25]. Still, all these models neglect Ohmic losses of the transmission lines. If Ohmic losses are included, the equations of motion become significantly more complex [10].

3 The nature and bifurcations of steady states

During steady operation of a power grid all nodes run with the grid's reference frequency Ω and fixed phase differences. A stable fixed point (i.e. equilibrium/steady state) of the equations of motion (20) describes the steady operation of the power grid. The loss of such a fixed point or a dynamical instability induce a desynchronization of the grid. Therefore, it is essential to understand the properties of the fixed points of the oscillator model, in particular their bifurcations and dynamical stability.

The fixed points of the equations of motion (20) are determined by the nonlinear algebraic equations

$$\forall j \in Z_N, \quad P_j + \sum_k K_{jk} \sin(\theta_k^* - \theta_j^*) = 0. \tag{31}$$

In the following, we present several results on the existence, stability and bifurcations of these fixed points, some aspects of which have been published for related systems in [26]. Fixed points are marked by an asterisk and the vector $\boldsymbol{\theta} = (\theta_1, \ldots, \theta_N)^T \in \mathbb{S}^N$ collects the phases of all machines, where $\mathbb{S} = \{x \,|0 \leq x \leq 2\pi\}$. The local frequencies are referred to by $v_j = d\theta_j/dt$ or $\boldsymbol{v} = d\boldsymbol{\theta}/dt$, respectively.

Lemma 1. *The network dynamics of the system defined by* (20) *and* (21) *for* $\alpha_j = 0$ *(zero damping) is a Hamiltonian system of the form*

$$\dot{\theta}_j = \frac{\partial \mathcal{H}}{\partial v_j}, \qquad \dot{v}_j = -\frac{\partial \mathcal{H}}{\partial \theta_j}, \tag{32}$$

where the phase θ_j *and the phase velocity*

$$v_j = d\theta_j/dt \tag{33}$$

are canonically conjugate variables for all $j \in Z_N$*. The Hamiltonian function has the natural form*

$$\mathcal{H}(\boldsymbol{v}, \boldsymbol{\theta}) = T(\boldsymbol{v}) + V(\boldsymbol{\theta}) \tag{34}$$

with the kinetic and potential energies

$$T(\boldsymbol{v}) = \frac{1}{2} \sum_j v_j^2 \tag{35}$$

$$V(\boldsymbol{\theta}) = -\sum_j P_j \theta_j - \frac{1}{2} \sum_{i,j} K_{ij} \cos(\theta_i - \theta_j). \tag{36}$$

Proof. Let $\mathcal{H}(\boldsymbol{v}, \boldsymbol{\theta}) = T(\boldsymbol{v}) + V(\boldsymbol{\theta})$ be a Hamiltonian function defined by (34), (35) and (36). Then $\mathcal{H}$ is continuously differentiable on any open star-shaped subset of the phase space with

$$\partial \mathcal{H}/\partial v_j = v_j = \dot{\theta}_j \tag{37}$$

and

$$\frac{\partial \mathcal{H}}{\partial \theta_j} = -P_j - \frac{1}{2} \sum_k \sum_l K_{kl} \frac{\partial}{\partial \theta_j} \cos(\theta_k - \theta_l) \tag{38}$$

$$= -P_j - \sum_k K_{jk} \sin(\theta_k - \theta_j). \tag{39}$$

Where the last equality follows from symmetry (21). Substituting (33), (37) and (39) into the Hamilton Eq. (32), the claim follows. □

Corollary 1. *The set of all fixed points of the oscillator Eqs.* (20) *and* (21) *for arbitrary* $\alpha_j \in \mathbb{R}$, $j \in Z_N$, *is identical to the set of fixed points of the Hamiltonian system* (32) *with* (34) *and* (33). *The fixed points are local extrema/saddle points of the potential function* $V(\boldsymbol{\theta})$ *(cf. also [27]).*

Proof. The set of fixed points of (32) is given by

$$P_{\text{Hamilton}} = \left\{ (\boldsymbol{\theta}^*, \boldsymbol{v}^*) \middle| \forall j \in Z_N, \quad \frac{\partial \mathcal{H}}{\partial v_j} = 0 \wedge -\frac{\partial \mathcal{H}}{\partial \theta_j} = 0 \right\}. \tag{40}$$

The set of fixed points of the oscillator Eq. (20) is given by

$$P_{\text{osc}} = \left\{ (\boldsymbol{\theta}^*, \boldsymbol{v}^*) = (\boldsymbol{\theta}^*, \mathbf{0}) \middle| \forall j \in Z_N, P_j + \sum_{k=1}^{N} K_{jk} \sin(\theta_k^* - \theta_j^*) = 0 \right\}, \tag{41}$$

independent of all α_j. If the transmission capacities are symmetric (21), the Hamiltonian and the original oscillator dynamics in the $\alpha_j = 0$ case are equivalent (have identical trajectories) as ensured by Lemma 1. Thus in particular their fixed points are identical. And since the fixed points of the oscillator model don't depend on α_j as per (41), the fixed points of the oscillator model for arbitrary α_j are also, by extension, identical to those of the Hamiltonian system.

As $T(\boldsymbol{v})$ is independent of all θ_j we have at each fixed point $(\boldsymbol{\theta}^*, \boldsymbol{v}^*)$ that

$$\left.\frac{\partial \mathcal{H}(\boldsymbol{v}, \boldsymbol{\theta})}{\partial \theta_j}\right|_{\boldsymbol{\theta}^*} = \left.\frac{\partial V(\boldsymbol{\theta})}{\partial \theta_j}\right|_{\boldsymbol{\theta}^*} = 0 \tag{42}$$

for all j such that the fixed points are located at local extreme/saddle points of V, demonstrating the second claim. □

Because of this correspondence, the theory of (damped) Hamiltonian dynamical systems (see [28] and references therein) helps us in characterizing the fixed points of the oscillator model and their bifurcations. We note that one has to be careful about the domain of $\mathcal{H}$. In principle, the phases are only defined modulo 2π but $\mathcal{H}$ is not 2π-periodic. This fact is not a major problem for our purpose, but it prohibits a definition of Gibbsian ensembles in statistical mechanics [19,27].

As shown in Corollary 1, the location of the fixed points $\boldsymbol{\theta}^* = (\theta_1^*, \ldots, \theta_N^*)$ is independent of the damping coefficients α_j. Furthermore, the location of the fixed point is the same for the celebrated Kuramoto [17–19] model such that our results may be adapted for this important model system. The question naturally arises: how do the stability properties of the fixed points change when α_j are varied or when we go from the oscillator model to Kuramoto model? We will answer this question subsequently, in Lemma 2 and Theorem 1.

The linear or spectral stability of a fixed point is obtained by linearizing the equations of motion. Writing

$$\boldsymbol{\xi} = \boldsymbol{\theta} - \boldsymbol{\theta}^* \tag{43}$$

the linearized equations of motion are given by

$$\frac{d}{dt}\begin{pmatrix} \dot{\boldsymbol{\xi}} \\ \boldsymbol{\xi} \end{pmatrix} = J \begin{pmatrix} \dot{\boldsymbol{\xi}} \\ \boldsymbol{\xi} \end{pmatrix}. \tag{44}$$

For the given damped oscillator system with equations of motion (20), the Jacobian is given by

$$J = \left(\begin{array}{c|c} -A_{N\times N} & -M_{N\times N} \\ \hline \mathbb{I}_{N\times N} & \mathbf{0}_{N\times N} \end{array}\right), \tag{45}$$

where

$$A = \begin{pmatrix} \alpha_1 & 0 & \cdots \\ 0 & \alpha_2 & \cdots \\ \vdots & \vdots & \ddots \end{pmatrix} \tag{46}$$

is a diagonal matrix specifying the damping coeeficient at each node and M is the Hesse matrix of the potential function $V(\boldsymbol{\theta})$ with elements

$$M_{ij} = \frac{\partial^2 V}{\partial\theta_i \partial\theta_j} \tag{47}$$

$$M = \begin{pmatrix} \sum_{l=1}^{N} K_{1l}\cos\left(\theta_1^* - \theta_l^*\right) & -K_{12}\cos\left(\theta_1^* - \theta_2^*\right) & \cdots \\ -K_{21}\cos\left(\theta_2^* - \theta_1^*\right) & \sum_{l=1}^{N} K_{2l}\cos\left(\theta_2^* - \theta_l^*\right) & \cdots \\ \vdots & \vdots & \ddots \end{pmatrix}. \tag{48}$$

This can be verified by a straightforward calculation.

Let λ_j be the eigenvalues of the Jacobian matrix J:

$$\forall j \in \{1, 2, \ldots, 2N\}, \quad J\boldsymbol{v_j} = \lambda_j \boldsymbol{v_j} \tag{49}$$

and let μ_k be the eigenvalues of the Hesse matrix M:

$$\forall k \in \{1, 2, \ldots, N\}, \quad M\boldsymbol{u_k} = \mu_k \boldsymbol{u_k}, \tag{50}$$

then we find the results stated below.

Lemma 2. *If $\mu_k \geq 0$ for all $k \in Z_N$, then $\Re(\lambda_j) \leq 0$ for all $j \in \{1, 2, \ldots, 2N\}$. Moreover, for each $\boldsymbol{v_j}$ such that $J\boldsymbol{v_j} = \mathbf{0}_{2N}$, there exists one and only one $\boldsymbol{u_k}$ such that*

$$M\boldsymbol{u_k} = \mathbf{0}_N \tag{51}$$

$$\boldsymbol{v_j} = (\underbrace{0, 0, \cdots, 0}_{\mathbf{0}_N}, \underbrace{u_1, u_2, \cdots, u_N}_{\boldsymbol{u_k}}) \tag{52}$$

$$:= \mathbf{0}_N \otimes \boldsymbol{u_k}. \tag{53}$$

Proof. Suppose $\boldsymbol{v} = \boldsymbol{v_1} \otimes \boldsymbol{v_2} \in \mathbb{R}^N \otimes \mathbb{R}^N$ is an eigenvector of J with eigenvalue λ. Then we have:

$$\lambda \boldsymbol{v_1} = -A\boldsymbol{v_1} - M\boldsymbol{v_2} \tag{54}$$

$$\lambda \boldsymbol{v_2} = \boldsymbol{v_1}. \tag{55}$$

Substituting (55) in (54):

$$0 = M\boldsymbol{v_2} + \lambda A\boldsymbol{v_2} + \lambda^2 \boldsymbol{v_2} \tag{56}$$

$$0 = \boldsymbol{v_2}^\dagger M\boldsymbol{v_2} + \boldsymbol{v_2}^\dagger A\boldsymbol{v_2}\lambda + \boldsymbol{v_2}^\dagger \boldsymbol{v_2}\lambda^2 \tag{57}$$

$$= \kappa_1^2 + \kappa_2^2\lambda + \kappa_3^2\lambda^2, \tag{58}$$

where

$$\kappa_1^2 = \boldsymbol{v_2}^\dagger M\boldsymbol{v_2} \geq 0, \quad (\text{M is positive semi} - \text{definite}) \tag{59}$$

$$\kappa_2^2 = \boldsymbol{v_2}^\dagger A\boldsymbol{v_2} \geq 0, \quad (\alpha_j \geq 0) \tag{60}$$

$$\kappa_3^2 = \boldsymbol{v_2}^\dagger \boldsymbol{v_2} \geq 0, \tag{61}$$

such that

$$\lambda = \frac{-\kappa_2^2 \pm \sqrt{\kappa_2^4 - 4\kappa_1^2\kappa_3^2}}{2\kappa_3^2}. \tag{62}$$

This implies $\Re(\lambda) \leq 0$, which proves the first part of the Lemma. Moreover, $\Re(\lambda) = 0 \iff \kappa_1^2 = 0$, which happens only if $M\boldsymbol{v_2} = 0$. This can be checked by expanding $\boldsymbol{v_2}$ in the eigenbasis of M. This proves the second part. □

Using the technical results presented above, we now analyze the stability and bifurcations in more detail. We show that stability is entirely determined by the Hesse matrix M and independent of the damping coefficients α_j. In many cases, M can be interpreted as a Laplacian matrix [29], such that the stability can be analyzed in terms of the topology of the grid.

Before we proceed, we note that by construction the Hesse matrix M has one zero eigenvalue (proof in Corollary 4) with the eigenvector:

$$\boldsymbol{u_1} = (1, 1, \cdots, 1) \tag{63}$$

$$M\boldsymbol{u_1} = \boldsymbol{0}. \tag{64}$$

For notational convenience we denote the eigenvalues of M sorted in ascending order of absolute values: $0 = |\mu_1| \leq |\mu_2| \leq |\mu_3| \leq \cdots \leq |\mu_N|$.

Theorem 1. *Let $\boldsymbol{\theta^*}$ be a fixed point of the oscillator model (20). Then $\boldsymbol{\theta^*} + \Delta(1, 1, \cdots, 1)^T$ is also a fixed point for all $\Delta \in \mathbb{R}$. If $\mu_j > 0$ for all $j \in \{2, 3, \ldots, N\}$, then the fixed point is transversely asymptotically stable.*

Proof. If $\mu_j > 0$ for all $j \in \{2, 3, \ldots, N\}$, Lemma 2 shows that the Jacobian J will have only one zero eigenvalue. We can see from (63) that the eigenvector corresponding to zero eigenvalue is

$$\boldsymbol{v^*} = \boldsymbol{0}_N \otimes (1, 1, \cdots, 1). \tag{65}$$

This eigenvector implies that a perturbation around a fixed point in the direction

$$\Delta\dot{\theta}_j^* = 0, \quad \Delta\theta_j^* = \text{constant} \tag{66}$$

is neutrally stable. However, this is simply due to the fact that the equations of motion (20) remains unchanged on adding a uniform global shift to the phase angles θ_j.

Since all other eigenvalues of the Jacobian J are less than 0, as guaranteed by Lemma 2, we see that all small perturbations transverse to the global shift (66) decay to zero with time. Transverse asymptotic stability therefore follows from the center manifold theorem (cf. [30]). □

Lemma 3. *A stable fixed point of the oscillator model (20) can be lost only via an inverse saddle-node bifurcation where one of the μ_j as defined in (50) becomes zero.*

Proof. To analyze the nature of bifurcations consider first the hamiltonian limit $\alpha_j = 0$. In a hamiltonian system only two types of bifurcation are possible when a parameter is varied smoothly [28]: a saddle-node bifurcation or a Krein bifurcation. At a Krein bifurcation complex quadruplets of eigenvalues emerge. However, this is impossible for the given dynamical system as eigenvalues of the Jacobian J are always purely real or purely imaginary for $\alpha = 0$, as demonstrated in (62). Thus the only possible bifurcation scenario is that of a saddle-node bifurcation. As the position (Theorem 1) and stability properties (Lemma 2) of fixed points are both independent of α_j the bifurcation remains the same also for the non-Hamiltonian case $\alpha_j > 0$. □

We note that in the Hamiltonian limit $\alpha = 0$ stability always means neutral stability. A minimum of the potential function $V(\boldsymbol{\theta})$ is an "elliptic fixed point" or "center" of the dynamical system as all eigenvalues of the Jacobian are purely imaginary. For $\alpha_j > 0$ all eigenvalues of the Jacobian acquire a negative real part, such that the fixed point becomes asymptotically stable.

We note that Theorem 1 also implies that the fixed points of the oscillator model share identical position and linear stability properties with the famous Kuramoto model [19] because $-M$ happens to be the Jacobian of the Kuramoto system.

4 Elementary example

To illustrate the mathematical results of the previous section, we first consider the simplest non-trivial grid, a two-element system consisting of one generator and one consumer. We assume that the power is balanced, i.e. $-P_1 = P_2$ and damping is uniform, i.e. $\alpha_1 = \alpha_2 = \alpha$. Therefore, $\ddot{\theta_1} + \ddot{\theta_2} = -\alpha(\dot{\theta_1} + \dot{\theta_2})$ and the mean phase $\theta_1 + \theta_2$ of the grid reaches a constant value exponentially in time. We thus consider only the dynamics of the phase difference $x = \theta_2 - \theta_1$. With $\Delta P = P_2 - P_1$ the equation of motion for this system reads

$$\frac{d^2x}{dt^2} = \Delta P - \alpha \frac{dx}{dt} - 2K \sin(x). \tag{67}$$

As the phase difference is defined modulo 2π, the phase space is cylindrical, $(\dot{x}, x) \in \mathbb{R} \times 2\pi\mathbb{S}^1$ (however, for illustration purposes and for comparing to the Hamiltonian case, it might be helpful to "unravel" the cylinder, i.e. assume that phases can take arbitrary values in $\mathbb{R}$).

Two fixed points exist for $2K > \Delta P$. The physical reason is that a steady operation of the grid is possible only when the transmission capacity of the line is larger than the power that must be transmitted. The location of the two fixed points $F_k = (x^*, \dot{x}^*)$ are specified by the conditions $\dot{x}^* = 0, \ddot{x}^* = 0$. The eigenvalues of the Jacobian at these points are given by

$$F_1 : \; x^* = \arcsin \frac{\Delta P}{2K} \tag{68}$$

$$\lambda_{\pm}^{(1)} = -\frac{\alpha}{2} \pm \sqrt{\left(\frac{\alpha}{2}\right)^2 - 2K \cos\left(\arcsin \frac{\Delta P}{2K}\right)} \tag{69}$$

$$F_2 : \; x^* = \pi - \arcsin \frac{\Delta P}{2K} \tag{70}$$

$$\lambda_{\pm}^{(2)} = -\frac{\alpha}{2} \pm \sqrt{\left(\frac{\alpha}{2}\right)^2 + 2K \cos\left(\arcsin \frac{\Delta P}{2K}\right)}. \tag{71}$$

The fixed point F_1 is stable: Depending on α, the eigenvalues are either both real and negative or complex with negative real values. The fixed point F_2 is a saddle, as $\lambda_+^{(1)}$ is always real and positive while $\lambda_-^{(1)}$ is always real and negative.

At $2K = \Delta P$ these two fixed points vanish in an inverse saddle-node bifurcation. No steady operation is possible for $2K < \Delta P$ as the load exceeds the capacity of the link. The nature of this bifurcation becomes most obvious when we consider the potential function introduced in the Hamiltonian formulation (36). The dynamical

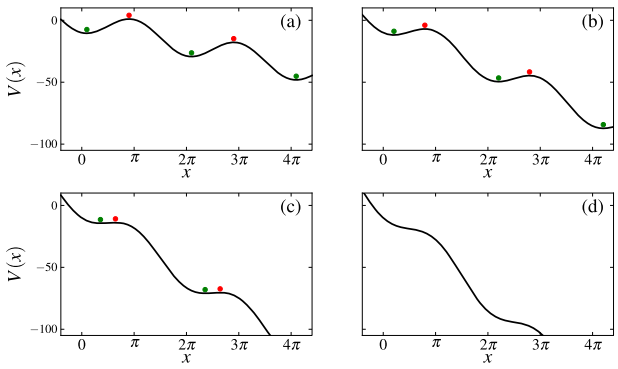

Fig. 1. The tilted washboard potential (73) for $K = 5$ and (a) $\Delta P = 3$, (b) $\Delta P = 6$, (c) $\Delta P = 9$ and (d) $\Delta P = 12$, respectively. The green (red) points illustrate the local minima (maxima) of the potential determining the location of a stable (unstable) fixed point.

system (67) can be viewed as the equation of motion of a mechanical particle moving in a tilted washboard potential with friction

$$\frac{d^2x}{dt^2} = -\alpha\frac{dx}{dt} - \frac{dV(x)}{dx} \tag{72}$$

$$\text{with } V(x) = -\Delta P x - K\cos(x). \tag{73}$$

The tilted washboard potential $V(x)$ and the critical points are illustrated in Fig. 1. When the tilting ΔP is increased, maxima and minima approach each other. At $\Delta P = 2K$ the critical points collide and vanish in an inverse saddle-node bifurcation, as previously explained by the form of the eigenvalues (68). This mechanical analog has been analyzed in great detail in statistical physics (see [31,32] and references therein).

5 Local vs. global stability

How about the *global* stability? Here we focus on the mathematical aspects of global stability and confine ourselves to the elementary example introduced in the previous section. Numerical studies for large complex networks were recently presented in [16,33].

The global stability properties of the two-element grid are summarized in the parametric portrait in Fig. 2, cf. also [31]. For $\Delta P > 2K$, there is no fixed point as discussed above. All trajectories converge to the global attractor – a limit cycle representing a run-away solution. For $\Delta P < 2K$ and strong damping, the stable fixed point F_1 is a global attractor. For weak damping, there exists a stable limit cycle, which coexists with the stable fixed point. The system will converge to either of them, depending on which basin of attraction the initial conditions belong to. This weak damping regime characterizes regular power grid operation such that the coexistence might be typical of real world power grids.

The critical damping $\alpha_c(\Delta P, K)$ is defined by the boundary that separates these two regions in the parametric portrait. At the boundary, the limit cycle emerges from a homoclinic orbit of the saddle fixed point in a homoclinic bifurcation, as illustrated in Fig. 3. Along the homoclinic orbit, the phase x increases 2π. The boundary intersects the saddle-node bifurcation line ($\Delta P = 2K$) at a numerically determined

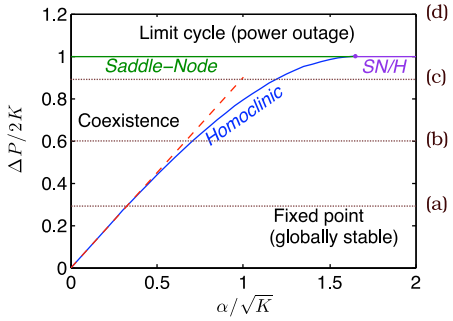

Fig. 2. Global stability phase diagram in parameter space for an elementary power grid consisting of one generator and one consumer (cf. [32]). The dashed red line shows the approximate phase boundary (85) in the case of low friction α. The dotted horizontal lines labelled by letters indicate the parameter values at which the potential V has been drawn in Fig. 1.

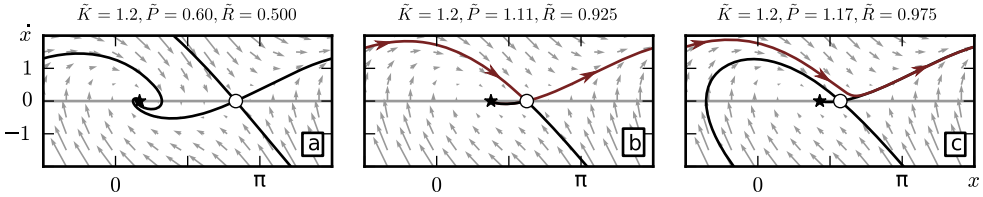

Fig. 3. Homoclinic bifurcation from globally stable fixed point to coexistence of limit cycle and fixed point in the two-element system. Black lines indicate the stable/unstable manifolds of the fixed points, brown lines indicate the homoclinic orbit. (a) In the globally stable region all trajectories converge to the stable focus ($\star$). (b) At the bifurcation, a homoclinic orbit (brown) is attached to the saddle ($\circ$). (c) The coexistence region. One unstable manifold of the saddle extends to the limit cycle, which has emerged from the homoclinic orbit. Parameters are: $\widetilde{K} = \frac{2K}{\alpha^2}, \widetilde{P} = \frac{\Delta P}{\alpha^2}, \widetilde{R} = \frac{\Delta P}{2K}$.

value of $\frac{\alpha}{\sqrt{K}} \approx 1.69$. For $\frac{\alpha}{\sqrt{K}} \gtrsim 1.69$, the saddle-node bifurcation and the homoclinic bifurcation combine to a saddle-node homoclinic bifurcation (cf. [34], Fig. 7.2).

An analytical approximation for the border between the globally stable and the coexistence regime can be obtained in the low-friction limit [32]. In order to determine stability criteria according to Lyapunov's second method [35], we define the energy E of the system as

$$E = \frac{(\dot{x})^2}{2} - 2K\cos(x). \tag{74}$$

It is to be noted that this energy E is not identical with the Hamiltonian H since this does not include the tilting introduced by the damping α. The change of energy is thus

$$\frac{dE}{dt} = \ddot{x}\dot{x} + 2K\sin(x)\dot{x}. \tag{75}$$

Inserting Eqs. (67) into (75) yields

$$\frac{dE}{dt} = (\Delta P - 2K\sin(x) - \alpha\dot{x})\,\dot{x} + 2K\sin(x)\dot{x} \tag{76}$$

$$= \Delta P\dot{x} - \alpha(\dot{x})^2. \tag{77}$$

If the average energy over one full period T decreases for all initial conditions for all time, the system is in the globally stable regime. The condition for the border between the globally stable and the coexistence regime is therefore described by:

$$\overline{\frac{dE}{dt}}^T = 0. \tag{78}$$

Hence

$$\Delta P \overline{\dot{x}}^T - \alpha \overline{\dot{x}^2}^T = 0 \tag{79}$$

is the condition for the border between the globally stable and the coexistence regime.

We can now calculate

$$\overline{\dot{x}}^T = \frac{1}{T}\int_0^T \dot{x}dt = \frac{1}{T}\int_{-\pi}^{\pi} dx = \frac{2\pi}{T} \tag{80}$$

and

$$\overline{\dot{x}^2}^T = \frac{1}{T}\int_0^T \dot{x}^2 dt = \frac{1}{T}\int_{-\pi}^{\pi} \dot{x}dx \tag{81}$$

$$= \frac{1}{T}\int_{-\pi}^{\pi} \sqrt{2E(x,\dot{x}) + 4K\cos(x)}dx. \tag{82}$$

Inserting Eq. (79), we get

$$\Delta P \frac{2\pi}{T} = \frac{\alpha}{T}\int_{-\pi}^{\pi} \sqrt{2E(x,\dot{x}) + 4K\cos(x)}dx. \tag{83}$$

At the parameters where a globally stable fixed point loses global stability, there will exist a trajectory of x which will satisfy $\dot{x} = 0$ at each successive peak of the potential landscape (cf. Fig. 1). Therefore we have $E_{\text{peak}} = 2K$. At the low friction approximation, we can neglect energy dissipation and hence assume E to be constant throughout the period. So we substitute $E(x,\dot{x}) = 2K$ in (83):

$$\int_{-\pi}^{\pi} \sqrt{4K + 4K\cos(x)}dx = 8\sqrt{2K}. \tag{84}$$

We thus find for the low-friction approximation the following border between the globally stable and the coexistence regime (cf. (83))

$$\Delta P = \tfrac{4\sqrt{2}}{\pi} \cdot \alpha\sqrt{K}. \tag{85}$$

The excellent agreement of the low-friction approximation (red line) for $\alpha/\sqrt{K} < 0.6$ with the numerically calculated border (blue curve) separating the two regimes is illustrated in Fig. 2.

6 Instabilities with and without overload

The regular operation of a power grid is described by a stable fixed point of the oscillator model (20). When a parameter, such as the power P_j or the transmission capacity K_{jk}, is varied smoothly, in some cases this fixed point can be lost, which signals an eventual desynchonization of the grid. If the local frequency deviates from

the reference Ω by more than a fixed security margin (typically 200 mHz, cf. [36]), an emergency shutdown is carried out which can lead to a large-scale power outage (see, e.g., [37–39]). In this section we discuss the physical aspects of this instability.

We first note that a stable fixed point can be lost only via a saddle-node bifurcation as described by Lemma 3. The fixed point is stable iff the real part of all eigenvalues of the Jacobian is smaller than or equal to zero. The bifurcation thus occurs when

$$\Re(\lambda_{\ell\pm}) \to 0 \qquad \Leftrightarrow \qquad \mu_\ell \to 0. \tag{86}$$

for any $\ell \in \{2, \ldots, N\}$. We recall that $\mu_1 = 0$, which corresponds to a global shift of the phases θ_j, has no physical significance.

Interestingly, the loss of a stable fixed point is generally *not* equivalent to an overload of one or more transmission lines. In particular, we can distinguish two different scenarios.

6.1 In normal operation, instability implies overload

When a power grid is only weakly loaded, the phase differences along each edge remain small. The power flow over the transmission line (j, k) increases monotonically with the phase difference as long as $|\theta_j - \theta_k| \leq \pi/2$ (cf. Eq. (15)). If this condition holds for all edges in the network, the grid is dynamically stable, as proved in Corollary 2 below, and we can find a direct graph theoretic interpretation of any bifurcation. We call this *normal operation*.

Corollary 2. *A fixed point is stable if $|\theta_i^* - \theta_j^*| \leq \pi/2$ holds for all edges (i, j) of the network.*

Proof. We define the *residual capacity* of each transmission line as

$$K_{ij}^{\text{red}} = K_{ij} \cos(\theta_j - \theta_i). \tag{87}$$

If $|\theta_i^* - \theta_j^*| \leq \pi/2$ holds for all edges, then $\forall i, j \in Z_N$

$$\begin{aligned} 0 &\geq K_{ij} \cos(\theta_i^* - \theta_j^*) && (88)\\ &= K_{ij} \sqrt{1 - \sin^2(\theta_j - \theta_i)} \\ &= \sqrt{K_{ij}^2 - F_{ij}^2} && (89) \end{aligned}$$

where $F_{ij} = K_{ij} \sin(\theta_j - \theta_i)$ is the power flow from node j to node i. Let us define a meta-graph $\widetilde{G}$ with the same set of vertices and edges as the original power grid, but with edge weights $w_{ij} = K_{ij}^{\text{red}}$. The Hesse matrix M as defined in (48) then becomes the Laplacian matrix of the meta-graph (details in Appendix 7). It is a well known result [29] that the eigenvalues of the Laplacian of a graph with *non-negative* edge weights satisfy:

$$0 = \mu_1 \leq \mu_2 \leq \cdots \leq \mu_N. \tag{90}$$

Stability of the fixed point directly follows from theorem 1. □

Corollary 3. *If $|\theta_i^* - \theta_j^*| \leq \pi/2$ holds for all edges (i, j), then whenever a fixed point undergoes a bifurcation, all connections between two components of the grid will become fully loaded.*

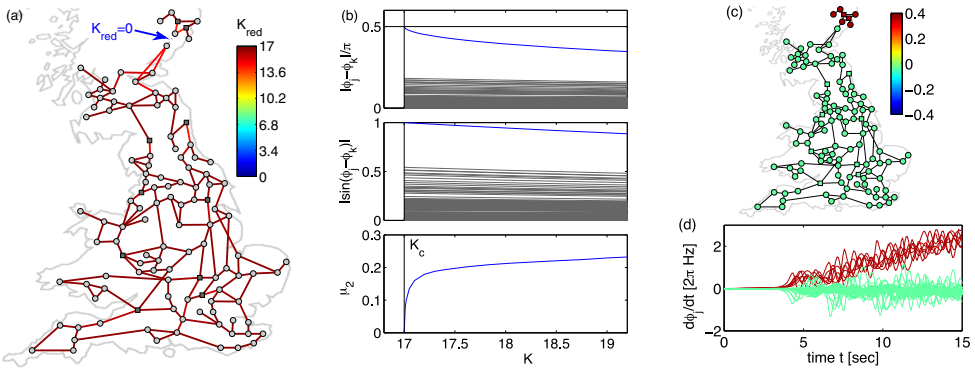

Fig. 4. Bifurcation due to an isolated overload. At the bifurcation the marked edge becomes overloaded and the meta-graph $\widetilde{G}$ decomposes into two fragments. (a) Model network based on the topology of the British high-voltage transmission grid [11,40]. Ten out of 120 nodes are randomly chosen to be generators with $P_j = +11\mathrm{s}^{-1}$ (□), all others have $P_j = -1\mathrm{s}^{-1}$ (○). All edges have the same transmission capacity K. The color code shows K^{red} defined in (87) at the bifurcation $K = K_c$. (b) The second eigenvalue μ_2 of the matrix M, the phase difference $\theta_j - \theta_k$ and the load $\sin(\theta_j - \theta_k)$ for all edges as a function of the transmission capacity K. At the bifurcation exactly one edge (marked in panel (a)) is fully loaded, $\theta_j - \theta_k = \pi/2$. (c) The Fiedler vector $\boldsymbol{v}_2$ at the bifurcation. (d) Dynamical instability after reducing the transmission capacity to $K = 0.98 \times K_c$. The color coding of the nodes is the same as in panel (c).

Proof. As shown in Corollary 2, if $|\theta_i^* - \theta_j^*| \leq \pi/2$ holds for all edges (i, j), then M is the Laplacian of the meta graph $\widetilde{G}$. It is shown in Corollary 4 that the multiplicity of the eigenvalue 0 in a graph's Laplacian equals the number of connected components of the graph [41,42].

Theorem 1 tells us that any bifurcation of a fixed point will be accompanied by one more eigenvalue of the Hesse matrix M becoming 0, which implies $\widetilde{G}$ splitting into one more component. This is equivalent to all edges between the components becoming fully loaded:

$$|F_{ij}| = K_{ij} \quad \Longleftrightarrow \quad K_{ij}^{\mathrm{red}} = 0. \tag{91}$$

□

An example for such a bifurcation is shown in Fig. 4 for a model grid based on the topology of the British high-voltage transmission grid [11]. The second eigenvalue μ_2 indicating dynamical stability is decreasing with decreasing transmission capacity K and vanishes at the bifurcation point $K = K_c$. At the bifurcation a single edge connecting the north of Scotland to the rest of the grid is fully loaded, $\theta_j - \theta_k = \pi/2$, such that the meta-graph $\widetilde{G}$ gets disconnected. Physically speaking, the fixed point is lost because of transmission line overload.

When the fixed point is lost for $K < K_c$, the disconnected components lose synchrony with each other. The components may remain synchronous internally, as depicted in Fig. 4c, where the two components, colored green and red, diverge from each other with time, but the frequencies within each component remain close.

The two components are readily identified by the eigenvector $\boldsymbol{v_2}$ associated with μ_2, the so-called Fiedler vector [29,43,44]:

$$M\boldsymbol{v_2} = \mu_2 \boldsymbol{v_2}. \tag{92}$$

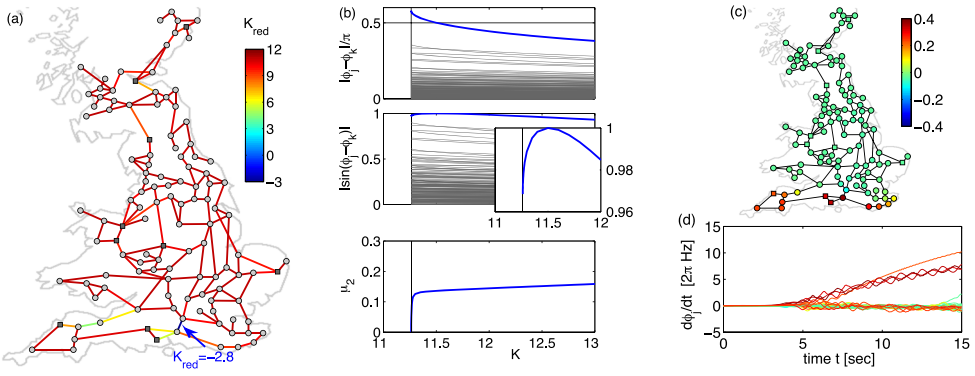

Fig. 5. Bifurcation without overload. At the bifurcation the marked edge is operating "beyond" an overload. (a) Model network based on the topology of the British high-voltage transmission grid [11,40]. Ten out of 120 nodes are randomly chosen to be generators with $P_j = +11\mathrm{s}^{-1}$ (□), all others have $P_j = -1\mathrm{s}^{-1}$ (○). All edges have the same transmission capacity K. The color code shows K^{red} defined in (87) at the bifurcation $K = K_c$. (b) The second eigenvalue μ_2 of the matrix M, the phase difference $\phi_j - \phi_k$ and the load $\sin(\phi_j - \phi_k)$ for all edges as a function of the transmission capacity K. At the bifurcation one edge (marked by an arrow in panel (a)) is operating beyond overload $|\phi_j - \phi_k| > \pi/2$. (c) The Fiedler vector $\boldsymbol{v}_2$ at the bifurcation. (d) Dynamical instability after reducing the transmission capacity to $K = 0.98 \times K_c$. The color coding of the nodes is the same as in panel (c).

When $\widetilde{G}$ becomes disconnected at the bifurcation, the Fiedler vector is given by

$$\boldsymbol{v_2} = \frac{1}{\sqrt{N_1 + N_2}} \Big(\underbrace{\sqrt{N_2/N_1}, \ldots}_{N_1 \text{ times}}, \underbrace{-\sqrt{N_1/N_2}, \ldots}_{N_2 \text{ times}}\Big)^T, \tag{93}$$

assuming that the nodes are labeled such that the first component is given by $1, \ldots, N_1$ and the second by $N_1+1, \ldots, N_1+N_2$. The Fiedler vector thus predicts the dynamics when stability is lost as shown in Fig. 4d.

6.2 Instability without overload

A different scenario can occur when the condition $|\theta_i^* - \theta_j^*| \leq \pi/2$ is not satisfied for one or more edges. This is possible for a stable fixed point in complex networks at the edge of the stable parameter region. Then we can have $K_{jk}^{\mathrm{red}} < 0$ such that the meta-graph is no longer a *non-negative* graph and the results discussed in the previous section do not apply.

In this case the bifurcation of a fixed point is generally *not* associated with any overload. In particular, the grid is already operating "beyond" an overload at the bifurcation point. An example of such a bifurcation is shown in Fig. 5. The marked edge has a phase difference of $|\theta_j^* - \theta_k^*| > \pi/2$ such that $K_{jk}^{\mathrm{red}} < 0$. The loss of stability is a collective effect of the entire grid and in particular there is no simple graph theoretical interpretation of the bifurcation. Consequently, the Fiedler vector defined in (92) only gives a limited insight into the desynchronization dynamics when the fixed point is lost.

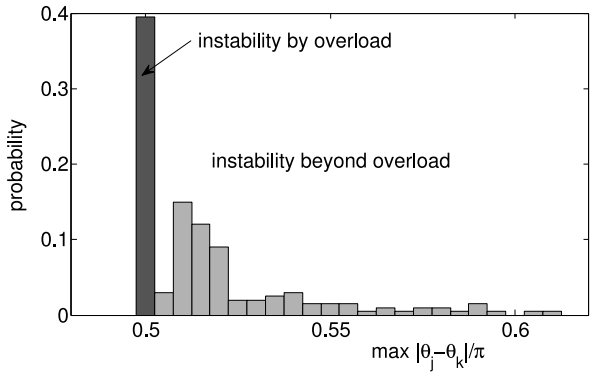

Fig. 6. Statistical analysis of the different bifurcation scenarios based on an ensemble of 200 different model networks. Shown is a histogram of the maximum phase difference $\max_{\text{edges}(j,k)} |\theta_j - \theta_k|$ at the bifurcation point. In approximately 40% of all realizations the steady state is lost because of an isolated overload as shown in Fig. 4. In approximately 60% of all realizations the grid is operating beyond an overload at the bifurcation point, i.e. $|\theta_j - \theta_k| > \pi/2$ for at least one edge, as shown in Fig. 5. Results have been obtained for 200 realizations of the model network based on the topology of the British power grid with random generator positions.

6.3 Relevance of bifurcation scenarios

The two bifurcation scenarios regularly occur in networks with complex topologies. We have analyzed the bifurcation for 200 realizations of the model network based on the topology of the British power grid with random generator positions (see Fig. 6). We find that the loss of the steady state is caused by an isolated overload in approximately 40% of the sample networks while the grid is operating beyond overload in the remaining 60% of all cases.

We note that the loss of a steady state and the following desynchronization generally leads to a large-scale power outage (cf. [37–39]). In current power grids this can happen only in periods of extreme loads while the phase difference is generally much smaller than $\pi/2$ in periods of average load. However, extreme loads are expected to become much more likely in the future if the power grid is not sufficiently adapted to the energy transition to renewable sources [3].

The two examples shown in Fig. 4 and Fig. 5 capture the essential mathematical aspects of this bifurcation for two model networks. Hence they are of interest both for fundamental research and as a guideline for the the analysis of real-world power grids though being simplified. In the figures we have illustrated the system stability for two model networks as a function of the parameter K in the very tradition of the physics literature on oscillator models (cf. [17–19] and references therein). In real world grids, the connectivity K_{ij} is generally fixed while generation and load can change strongly. As an essential parameter affecting stability is the transported power P *relative to* the connectivity K_{ij}, we vary K_{ij} to study qualitative changes in the collective dynamics of the network.

6.4 Braess' paradox

We finally note that a variety of parameter changes can induce a bifurcation. Stability can be lost due to an increase of the power load or the damage of a transmission line, but surprisingly also by *increasing* the transmission capacity or even by putting a new

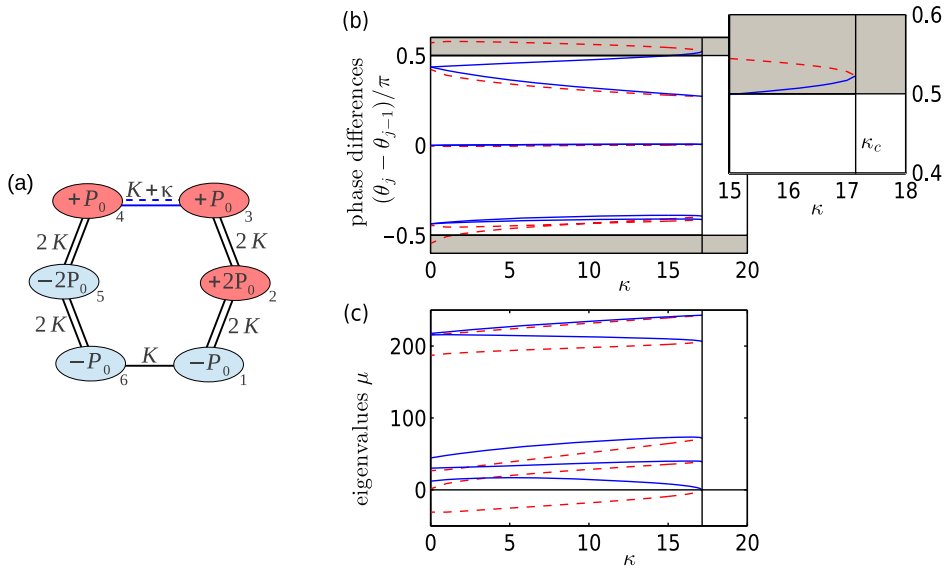

Fig. 7. Loss of stability due to the *increase* of local transmission capacity in a circular network. A stable (—) and an unstable (− − −) fixed point vanish in a saddle-node bifurcation at the critical point $\kappa_c = 17.15$. The stable fixed point (blue) is lost. (a) Topology of the network. The capacity of the upper edge $(3, 4)$ is increased by an amount κ. (b) Phase differences along the edges of the cycle. Close to the bifurcation, the phase difference $|\theta_5 - \theta_4|$ exceeds $\pi/2$ for the stable fixed point (see inset). (c) Eigenvalues of the Hesse matrix M, which yield the eigenvalues of the Jacobian via (62). Parameters are $K = 50$ and $P_0 = 49$.

line into operation. Figure 7 shows an example of this effect called Braess' paradox [45]. A detailed discussion of Braess' paradox in supply networks is presented in [12,46].

In this example (Fig. 7) the stable fixed point ceases to exist after a saddle node bifurcation when the capacity of the upper transmission line is increased to a critical value $\kappa > \kappa_c = 17.15$. Again, we find that the grid is no longer in normal operation in the vicinity of the bifurcation as the phase difference $\theta_5^* - \theta_4^*$ exceeds $\pi/2$ already for $\kappa > 15.2$. This constitutes a clear example that adding lines or improving line capacities may also induce instabilities without overloads via Braess' paradox [12,46].

7 Conclusions and discussion

How can supply networks become unstable? In simple systems where the loads are the only relevant variables, the answer is simple: instabilities emerge if and only if one or more elements overload, cf. also [47].

As we intended, we have demonstrated in this article how instability can also emerge in the absence of any overloads. We have explicated stability conditions for fixed points (steady operation) of oscillatory power grid models [9,11,13], where in addition to the pure flows, phase variables play a crucial role. We linked a Hamiltonian description to existence and bifurcation types of fixed points. In particular, we demonstrated that instabilities may emerge with and without transmission line overloads and that – through Braess' paradox [12,46] – adding new lines may also create collective instabilities without line overloads.

Like the coupled phase oscillator model described here in the context of power grids, the function of many physical and biological supply networks depends on and involves quantities other than the network load. A notable example from biology is leaf vasculature and stomatal patchiness. Stomatal patchiness is the oscillatory dynamics of the opening and closing of patches of leaf stomata, which is believed to be the result of hydraulic and elastic coupling between neighbouring stomata. This dynamics can arise in a self organised manner in situations where a uniform stomatal aperture should be expected. Although recent progress has been made, stomatal patchiness is still not completely understood [48], especially in the context of the underlying hydraulic coupling of the stomata to the vascular system.

Similarly, the plant phloem is a dynamical transport system involving a number of interdependent quantities. The phloem vascular elements transfer sap (a sugar rich water solution) from and between the photo-synthesising tissues to the rest of the plant. Sugars are being loaded in the phloem actively or passively at the sites of photosynthesis and the rate of sugar production and loading (determining the vascular network operation) can vary from site to site. The sugar concentration is a field of independent variables coupled to the network load (phloem fluid flow), and depending on the loading regime, the system has a potential of a rich dynamical behaviour [49,50]. The plant phloem might thus constitute a biological candidate system where instabilities of normal supply function may emerge without overloads.

We acknowledge support from the Bundesministerium für Bildung und Forschung and by a grant of the Max Planck Society to M.T.

Appendix: A Properties of graph Laplacian

Definition 1. *Let G be a weighted graph with n nodes with all the edge weights $w_{ij} \geq 0$. The Laplacian M is an $N \times N$ matrix given by:*

$$M_{ij} = -w_{ij} + \delta_{ij} \sum_{k=1}^{N} w_{ik}. \tag{94}$$

Theorem 2. *In a fully connected graph G, the Laplacian L has exactly one zero eigenvalue.*

Proof. The Laplacian M obviously has one zero eigenvalue: the corresponding eigenvector being $\boldsymbol{v_0} = (1, 1, \cdots, 1)$:

$$\begin{aligned} (M\boldsymbol{v_0})_i &= \sum_j M_{ij} v_{0j} \\ &= \sum_j M_{ij} \\ &= \sum_j \left[\sum_k \delta_{ij} w_{ik} - w_{ij} \right] \\ &= 0. \end{aligned} \tag{95}$$

Suppose there is another eigenvector $\boldsymbol{v'}$ with eigenvalue 0. Then:

$$\begin{aligned} 0 &= \boldsymbol{v'}^T M \boldsymbol{v'} \\ &= \sum_{ij} v'_i M_{ij} v'_j \\ &= \sum_{ij} v'_i \left(\sum_k \delta_{ij} w_{ik} - w_{ij} \right) v'_j \\ &= \sum_j \left(\sum_k w_{jk} \right) v'^2_j - \sum_{ij} w_{ij} v'_i v'_j \\ &= \sum_{i<j} \left[\sqrt{w_{ij}} \left(v'_i - v'_j \right) \right]^2 . \end{aligned} \tag{96}$$

Therefore it follows that $\sqrt{w_{ij}}(v'_i - v'_j) = 0$ for all $i, j \in Z_N$. This implies whenever two nodes are connected by an edge ($w_{ij} \neq 0$), $v_i = v_j$. Now, by virtue of G being connected, $v'_i = v'_j$ must hold for all (i, j). But that implies $\boldsymbol{v'} = \boldsymbol{v_0}$, up to a multiplicative constant. □

Corollary 4. *The multiplicity of* 0 *eigenvalue in the Laplacian of a graph equals its number of connected components.*

Proof. For a graph with c connected components, if the node indices are chosen properly, the Laplacian L will be in a block diagonal form with c blocks. Then following the same reasoning as in Theorem 2, the result follows. □

References

1. E. Marris, Nature **454**, 570 (2008)
2. J.A. Turner, Science **285**, 687 (1999)
3. T. Pesch, H.-J. Allelein, J.-F. Hake, Eur. Phys. J. Special Topics **223**(12), 2561 (2014)
4. D. Heide, L. von Bremen, M. Greiner, C. Hoffmann, M. Speckmann, S. Bofinger, Renewable Energy **35**, 2483 (2010)
5. F. Böttcher, S. Barth, J. Peinke, Stoch. Environ. Res. Ris. Assess. **21**, 299 (2007)
6. P. Milan, M. Wächter, J. Peinke, Phys. Rev. Lett. **110**, 138701 (2013)
7. A.R. Bergen, D.J. Hill, IEEE Trans. Power Apparatus Syst. **PAS-100**, 25 (1981)
8. D. Hill, G. Chen, *Power systems as dynamic networks*, in Proc. of the 2006 IEEE International Symposium on Circuits and Systems (2006), p. 725
9. G. Filatrella, A.H. Nielsen, N.F. Pedersen, Eur. Phys. J. B **61**, 485 (2008)
10. J. Machowski, J. Bialek, J. Bumby, *Power system dynamics, stability and control* (John Wiley & Sons, New York, 2008)
11. M. Rohden, A. Sorge, M. Timme, D. Witthaut, Phys. Rev. Lett. **109**, 064101 (2012)
12. D. Witthaut, M. Timme, New J. Phys. **14**, 083036 (2012)
13. M. Rohden, A. Sorge, D. Witthaut, M. Timme, Chaos **24**, 013123 (2014)
14. F. Dörfler, M. Chertkov, F. Bullo, Proc. National Acad. Sci. **110**, 2005 (2013)
15. A.E. Motter, S.A. Myers, M. Anghel, T. Nishikawa, Nat. Phys. **9**, 191 (2013)
16. P.J. Menck, J. Heitzig, J. Kurths, H.J. Schellnhuber, Nat. Comm. **5** (2014)
17. Y. Kuramoto, *Self-entrainment of a population of coupled non-linear oscillators*, in International Symposium on Mathematical Problems in Theoretical Physics, edited by H. Araki (Springer, New York, 1975), Lecture Notes in Physics, Vol. 39, p. 420
18. S.H. Strogatz, Phys. D: Nonlinear Phenom. **143**, 1 (2000)
19. J.A. Acebrón, L.L. Bonilla, C.J. Pérez Vicente, F. Ritort, R. Spigler, Rev. Mod. Phys. **77**, 137 (2005)

20. P. Kundur, *Power System Stability and Control* (McGraw-Hill, New York, 1994)
21. Y. Susuki, I. Mezic, T. Hikihara, *Global swing instability of multimachine power systems*, in Decision and Control, CDC 2008, 47th IEEE Conference on (IEEE, 2008), p. 2487
22. Y. Susuki, I. Mezić, T. Hikihara, J. Nonlinear Sci. **21**(3), 403 (2011)
23. F. Dorfler, F. Bullo, Circ. Syst. I: Regul. Papers, IEEE Trans. **60**(1), 150 (2013)
24. A.R. Bergen, D.J. Hill, Power Appar. Syst., IEEE Trans. (1), 25 (1981)
25. K. Schmietendorf, J. Peinke, R. Friedrich, O. Kamps [arXiv:1307.2748] (2013)
26. H.D. Chiang, F.F. Wu, P.P. Varaiya, Circ. Syst., IEEE Trans. **34**(2), 160 (1987)
27. C.J. Perez, F. Ritort, J. Phys. A: Math. General **30**, 8095 (1997)
28. J. Howard, Scholarpedia **8**, 3627 (2013)
29. M.E.J. Newman, *Networks – An introduction* (Oxford University Press, Oxford, 2010)
30. H.K. Khalil, J. Grizzle, *Nonlinear Systems*, Vol. 3 (Prentice hall Upper Saddle River, 2002)
31. M. Levi, F.C. Hoppenstaedt, W.L. Miranker, Quart. Appl. Math. **36**, 167 (1978)
32. H. Risken, *The Fokker-Planck Equation* (Springer, Berlin Heidelberg, 1996)
33. P.J. Menck, J. Heitzig, N. Marwan, J. Kurths, Nat. Phys. **9**, 89 (2013)
34. Y. Kuznetsov, *Elements of Applied Bifurcation Theory*, Vol. 112 (Springer, 1998)
35. P.C. Parks, IMA J. Math. Contr. Inf. **9**(4), 275 (1992)
36. U. for the Co-ordination of Transmission of Electricity", *Continental Europe Operation Handbook* (2014)
37. P. Fairley, IEEE Spectr. **41**, 22 (2004)
38. U.S.-Canada Power System Outage Task Force, https://reports.energy.gov/BlackoutFinal-Web.pdf (2004)
39. Union for the Coordination of Transmission of Electricity, *Final Report on the System Disturbance on 4 November 2006*, http://www.entsoe.eu/~library/publications/ce/otherreports/Final-Report-20070130.pdf (retrieved 13/10/2009) (2007)
40. I. Simonsen, L. Buzna, K. Peters, S. Bornholdt, D. Helbing, Phys. Rev. Lett. **100**, 218701 (2008)
41. W.N. Anderson Jr., T.D. Morley, Linear Multilinear A **18**, 141 (1985)
42. B. Mohar, in *Graph Theory, Combinatorics, and Applications 2*, edited by Y. Alavi, G. Chartrand, O.R. Oellermann (Wiley, 1991), p. 871
43. M. Fiedler, Czechoslovak Math. J. **23**, 298 (1973)
44. S. Fortunato, Phys. Reports **486**, 75 (2010)
45. D. Braess, Unternehmensforschung **12**, 258 (1968)
46. D. Witthaut, M. Timme, Eur. Phys. J. B **86**, 377 (2013)
47. S.D. Pathak, J.M. Day, A. Nair, W.J. Sawaya, M.M. Kristal, Decision Sci. **38**(4), 547 (2007)
48. A.M.T. Ramos, C.P.C. Prado, Phys. Rev. E **87**, 012719 (2013), http://link.aps.org/doi/10.1103/PhysRevE.87.012719
49. K.H. Jensen, J. Lee, T. Bohr, H. Bruus, N. Holbrook, M. Zwieniecki, J. Royal Society Interface **8**(61), 1155 (2011)
50. J. Patrick, Ann. Rev. Plant Biol. **48**(1), 191 (1997)